

Theoretical study of differential cross sections for the ionization of helium by fast proton impact

M Mondal, B Mandal, T Mistry, D Jana, and M Purkait

Citation: Chin. Phys. B, 2024, 33 (**11**): 113401. DOI: 10.1088/1674-1056/ad74e6
Journal homepage: http://cpb.iphy.ac.cn; http://iopscience.iop.org/cpb

What follows is a list of articles you may be interested in

Absolute partial and total ionization cross sections of carbon monoxide with electron collision from 350 eV to 8000 eV

Taj Wali Khan, Weizhe Huang(黄伟哲), Enliang Wang(王恩亮), Xu Shan(单旭), and Xiangjun Chen(陈向军)
Chin. Phys. B, 2024, 33 (**4**): 043401. DOI: 10.1088/1674-1056/ad20dd

Theoretical investigation of electron-impact ionization of W^{8+} ion

Shiping Zhang(张世平), Fangjun Zhang(张芳军), Denghong Zhang(张登红), Xiaobin Ding(丁晓彬), Jun Jiang(蒋军), Luyou Xie(颉录有), Yulong Ma(马玉龙), Maijuan Li(李麦娟), Marek Sikorski, and Chenzhong Dong(董晨钟)
Chin. Phys. B, 2024, 33 (**3**): 033401. DOI: 10.1088/1674-1056/ad1487

Fragmentation dynamics of electron-impact double ionization of helium

Shiwei Liu(刘士炜), Difa Ye(叶地发), and Jie Liu(刘杰)
Chin. Phys. B, 2023, 32 (**6**): 063402. DOI: 10.1088/1674-1056/acbe33

Electron-impact ionization of W^{9+} and W^{10+}

Runjia Bao(鲍润家), Junkui Wei(魏军奎), Lei Chen(陈雷), Bowen Li(李博文), and Ximeng Chen(陈熙萌)
Chin. Phys. B, 2023, 32 (**6**): 063401. DOI: 10.1088/1674-1056/aca14d

Electron-impact ionization cross section calculations for lithium-like ions

Guo-Jie Bian(卞国杰), Jyh-Ching Chang(张稚卿), Ke-Ning Huang(黄克宁), Chen-Sheng Wu(武晨晟), Yong-Jun Cheng(程勇军), Kai Wang(王凯), and Yong Wu(吴勇)
Chin. Phys. B, 2022, 31 (**1**): 013401. DOI: 10.1088/1674-1056/ac229e

---

Theoretical study of differential cross sections for the ionization of helium by fast proton impact

M Mondal, B Mandal, T Mistry, D Jana, and M Purkait[†]

Department of Physics, Ramakrishna Mission Residential College, Narendrapur, Kolkata - 700103, India

(Received 20 June 2024; revised manuscript received 12 August 2024; accepted manuscript online 29 August 2024)

We present the angular distribution of the ejected electron for single ionization of He by fast proton impact. A four-body formalism of the three-Coulomb wave is applied to calculate the triple differential cross sections at several impact energies in the scattering, perpendicular and azimuthal planes. Moreover, the three-body formalism of three-Coulomb, two-Coulomb and first Born approximation models has also been used to study the many-body effect on electron emission and the validity of the models. In the three-Coulomb wave model, the final state wave function incorporates distortion due to the three-body mutual Coulombic interaction. In this formalism, we use an uncorrelated and correlated Born initial state, which consists of a plane wave for the incoming projectile times a two-electron bound state wavefunction of the helium atom representing the $1s^2(^1S)$ state. But, in the case of the three-body formalism, the initial state wavefunction consists of a long-range Coulomb distortion for the incoming projectile and one active electron of the He atom described by the Roothaan–Hartree–Fock wavefunction. The structure with a single or two peaks with unequal intensity is observed in the angular distributions of the triple differential cross sections for the different kinematic conditions. In addition, the influence of static electron correlations is investigated using different bound state wavefunctions for the ground state of the He target. In the four-body formalism, the present computations are very fast by reducing a nine-dimensional integral to a two-dimensional real integral. Despite the simplicity and speed of the proposed quadrature, the comparison shows that the obtained results are in reasonable agreement with the experiment and are compatible with those of other theories.

Keywords: ionization, cross sections, collision, atoms, ions

PACS: 34.70.+e **DOI:** 10.1088/1674-1056/ad74e6

1. Introduction

The study of ionization processes in atoms and molecules by fast ion impact is important in various areas of physics and chemistry. It is also a good topic for studying the dynamics of few-body collisions. In this context, triple differential cross sections (TDCSs) give us complete information on collision dynamics and provide the most sensitive tests of different theoretical models. Among various ion–atom collisions, single ionization of a He atom by proton impact is a more fundamental reaction, for several reasons. He is the simplest multi-electron atom in nature and the collision of a proton with He is a pure four-body problem, which allows examination of the validity of the theoretical formalisms. The collision dynamics depends on the kinematic parameters. Most of the theoretical work on this collision process was done in the scattering plane,[1–9] where a structure with two peaks has been found in the angular distribution of electron emission. In this context, several experiments[10–20] have also been performed on ion–atom collisions due to the remarkable progress of the cold target recoil ion momentum spectroscopy (COLTRIMS). This allows us to measure the three-dimensional angular distributions of the electrons ejected from atoms at given values of energy and momentum transfer. On the other hand, few theoretical works have been done on the TDCSs, either in the scattering, perpendicular[21–27] or azimuthal planes.[28] Therefore, the complete dynamics of single ionization of He in the ground state for different collision planes is more challenging, both theoretically and experimentally.

Many theoretical calculations have been carried out for this particular process based on the three-body model. For example, the first Born approximation (FBA),[19] the three-body distorted wave (3DW),[29–31] the continuum distorted-wave eikonal initial state (CDW-EIS),[10,23,32,33] convergent close coupling (CCC),[34] the three-Coulomb wave (3CW) or Brauner, Briggs and Klar (BBK) model[35–38] and the three-body distorted-wave eikonal initial state (3DW-EIS).[39] At the same time, a few four-body formalisms of different models have also been published for the calculation of the TDCS for single ionization of atoms by ion impact at intermediate and high impact energies. For example, the Glauber approximation,[8] the FBA with two-Coulomb wave (FBA-2CW),[21,22] corrected continuum wave,[2] plane-wave FBA,[15,40] 3CW[1,9,18,40,41] and CDW-EIS.[42] A frequently used model for single ionization of a multi-electron atom is the frozen core approximation. In this approximation, the ionized electron is considered active while the other electron is inactive. This electron does not change state during the collision, and can therefore be neglected in the calculation. The other important assumption in this approximation is that all the electrons in the atom are independent, and therefore the correlations between them can be ignored. This approximation is valid for high impact energies. On the other hand, correla-

[†]Corresponding author. E-mail: mpurkait_2007@rediffmail.com; rkmcnpur@gmail.com

© 2024 Chinese Physical Society and IOP Publishing Ltd

tion with the initial target atomic wavefunction is considered in the four-body model and may change the collision dynamics. Thus, the four-body model, with He as a target, represents a more physically accurate description for ion–atom collisions and it will give more information about collision dynamics. So, it may be expected that the four-body model will predict the experimental results better than the three-body model in a wide energy range. In Refs. [43–46], it is quite surprising that the four-body model showed worse agreement with the experiment than the three-body model. Ghanbari-Adivi and Velayali[47] studied the difference between three-body and four-body distorted wave models for the formation of positronium. Their study was primarily focused on the role of correlation in the ground state atomic wavefunction. A significant difference between the two sets of results was found. Recently, differential cross sections (DCSs) for capture of a single electron from He by bare ion impact were calculated using a frozen core three-body model and an active electron four-body model within the FBA.[48] Their investigation shows that the inclusion of electron correlation in the four-body model has a minimum effect on the DCS. However, in some cases, for example with B^{5+} as a projectile, both models predicted the experimental results very well.

This paper presents a theoretical study of the angular distribution of electron emission for the single ionization of He atoms in the ground state by proton impact for different kinematic conditions. Our primary focus is to trace any differences in the TDCSs by applying a 3CW model based on the three-body and four-body models (called 3CW-3B and 3CW-4B, respectively) in the scattering, perpendicular and azimuthal planes. The TDCSs are presented for H^+ projectile impact with energies of 0.5 MeV·amu^{-1}, 1 MeV·amu^{-1} and 2 MeV·amu^{-1}. Another motivation is the role of correlation in the target atomic wavefunction and the validity of the two models. This work is an extension of our previous work,[49] where the TDCSs were only calculated in the scattering plane at impact energies of 0.75 MeV and 1 MeV.

The paper is organized as follows. In Section 2, the theory of the two formalisms is presented and the partial transition amplitudes are evaluated. The obtained results are compared with experiments in Section 3. Finally, the concluding remarks are given in Section 4. Atomic units (a.u.) are used throughout unless otherwise noted.

2. Theoretical treatment

In the single ionization of a He atom, a proton of mass M_P and charge Z_P impacts with a He atom. One of the electrons in the target is ionized and the other electron remains bound to the He, forming He^+ $(n = 1)$. This electron does not change its quantum state, i.e., it is frozen, which screens the nucleus. As a result, the shape and magnitude of the TDCS results can be affected by the screening. Even the collision dynamics can be changed. Therefore, there are some differences observed in the angular distribution of the ejected electron between the frozen core and the active electron model. So, the projectile–frozen target nucleus interaction is changed, which plays an important role in the single ionization process. To study the differences between the three-body and four-body models, we use the exact form of the 3CW in the asymptotic region originally proposed by BBK.[35] The BBK model is used to study the mechanism of the ionization process. It mainly incorporates the pairwise mutual Coulomb interaction among three unbound charged particles. In the present work, this model determines the final channel wave function for 3CW-3B and 3CW-4B models. Here a brief outline of two theoretical models (3CW-3B and 3CW-4B) along with the FBA-2CW model based on the three-body model is given, where the interaction between the projectile and residual target ion (PI) and the post-collision interaction (PCI) are turned off.

2.1. Four-body three-Coulomb wave (3CW-4B)

The TDCS in a.u. is obtained from the following relation:

$$\mathrm{TDCS} = N_e (2\pi)^4 \frac{k_e k_s}{k_0} |F^{(-)}(\boldsymbol{q}, \boldsymbol{k}_e)|^2, \tag{1}$$

where $\boldsymbol{k}_0$, $\boldsymbol{k}_e$ and $\boldsymbol{k}_s$ are the momenta of the incoming projectile, ejected electron and scattered projectile, respectively. $\boldsymbol{q} = \boldsymbol{k}_0 - \boldsymbol{k}_s$ denotes the projectile momentum transfer and N_e is the number of indistinguishable electrons in the atomic shell. Here, $F^{(-)}(\boldsymbol{q}, \boldsymbol{k}_e)$ represents the prior form of the transition amplitude for single ionization of He by ion impact. The form of $F^{(-)}(\boldsymbol{q}, \boldsymbol{k}_e)$ is given by

$$\begin{aligned} &F^{(-)}(\boldsymbol{q}, \boldsymbol{k}_e) \\ &= \langle \chi_{3C}^{(-)}(\boldsymbol{r}_1, \boldsymbol{s}_1, \boldsymbol{R}) \phi_{He}^{+}(\boldsymbol{r}_2) | V_i^{4B} | \chi_i(\boldsymbol{R}) \phi_{He}(\boldsymbol{r}_1, \boldsymbol{r}_2) \rangle, \end{aligned} \tag{2}$$

where $\chi_i(\boldsymbol{R})$ is the incident projectile plane wave, $\phi_{He}(\boldsymbol{r}_1, \boldsymbol{r}_2)$ is the target atomic wavefunction, $\phi_{He}^{+}(\boldsymbol{r}_2)$ is the bound state of the residual He^+ ion $(n = 1)$ and $\chi_{3C}^{(-)}(\boldsymbol{r}_1, \boldsymbol{s}_1, \boldsymbol{R})$ represents the correlated wavefunction of the three unbound charged particles[35] in the final state. V_i^{4B} is the Coulomb interaction between the projectile and atom given by

$$V_i^{4B} = \left(\frac{2}{R} - \frac{1}{|\boldsymbol{r}_1 - \boldsymbol{R}|} - \frac{1}{|\boldsymbol{r}_2 - \boldsymbol{R}|} \right). \tag{3}$$

Here $\boldsymbol{r}_1$, $\boldsymbol{r}_2$ and $\boldsymbol{R}$ are the position vectors measured relative to the target nucleus for the two electrons in the atom and the projectile, respectively. The transition amplitude of Eq. (2) contains nine-dimensional integrals. Following Ref. [9], this integral is reduced to a two-dimensional real integral.

2.2. Three-body three-Coulomb wave (3CW-3B)

The second electron of the He atom remains in the ground state of the final ionic state He^+, i.e., it does not change the quantum state, therefore the inactive electron is neglected in

the calculation. This electron screens the target nucleus. Then, the three-body transition amplitude becomes

$$F^{(-)}(\boldsymbol{q},\boldsymbol{k}_{\rm e}) = \langle \chi_{\rm 3C}^{(-)}(\boldsymbol{r}_1,\boldsymbol{s}_1,\boldsymbol{R})|U_{\rm i}^{\rm 3B}|\chi_{\rm i}^{+}(\boldsymbol{R})\phi_{\rm He}(\boldsymbol{r}_1)\rangle, \quad (4)$$

where $U_{\rm i}^{\rm 3B} = \left(\frac{1}{R} - \frac{1}{|\boldsymbol{r}_1-\boldsymbol{R}|}\right)$. Here, $\phi_{\rm He}(\boldsymbol{r}_1)$ is the initial bound state wavefunction of He, where one active electron is described by the Roothaan–Hartree–Fock (RHF) wavefunction. This is a more sophisticated single-electron wavefunction and is given by

$$\phi_{\rm He}(\boldsymbol{r}_1) = \sum_{j=1}^{n} \xi_j \, {\rm e}^{-\delta_j r_1}, \quad (5)$$

where ξ_j and δ_j can be found in Ref. [50]. $\chi_{\rm i}^{+}(\boldsymbol{R})$ is the Coulomb distorted wave for the incident projectile and the corresponding distorted potential is $U_{\rm i}$. We note that $\chi_{\rm 3C}^{(-)}$ is the same for the three-body and four-body models. Equation (4) contains a six-dimensional integral which is reduced to three-dimensional integrals. All integrals are performed numerically using the Gauss–Legendre quadrature method.

2.3. Three-body two-Coulomb wave (2CW-3B)

In this approximation, the scattered projectile is treated as a plane wave and the ejected electron motion is influenced by both the projectile and the target ion. On the other hand, the initial state wavefunction remains the same as in the 3CW-3B model. So the transition amplitude is given by

$$F^{(-)}(\boldsymbol{q},\boldsymbol{k}_{\rm e}) = \langle \chi_{\rm 2C}^{(-)}(\boldsymbol{r}_1,\boldsymbol{s}_1)\chi_{\rm s}(\boldsymbol{R})|U_{\rm i}^{\rm 3B}|\chi_{\rm i}(\boldsymbol{R})\phi_{\rm He}(\boldsymbol{r}_1)\rangle. \quad (6)$$

2.4. Three-body first-Born approximation (FBA-3B)

In the FBA calculations, only the interaction between the electron leading to ejection and the target is accounted for. This is a one-center calculation. Therefore,

$$F^{(-)}(\boldsymbol{q},\boldsymbol{k}_{\rm e}) = \langle \chi_{\rm 1C}^{(-)}(\boldsymbol{r}_1)\chi_{\rm s}(\boldsymbol{R})|U_{\rm i}^{\rm 3B}|\chi_{\rm i}(\boldsymbol{R})\phi_{\rm He}(\boldsymbol{r}_1)\rangle. \quad (7)$$

In the FBA, both the PI interaction and PCI are absent.

Special attention has been given to convergence during the numerical integration of the transition amplitude that contains a function $f(\tau) = \tau^{{\rm i}\gamma-1}(1-\tau)^{-{\rm i}\gamma}$ by transforming a confluent hypergeometric function to complex contour integration.[9,51] Here γ is a Sommerfeld parameter that becomes very small with increasing velocity of the scattered proton and the ejected electron. As a result, the function is more oscillatory. However, the consequences of the three-dimensional integral for the three-body model and the two-dimensional integral for the four-body model are tested properly and the results presented here are correct up to an accuracy of 0.1%. For the three-body formalism, the three-dimensional integral comprises two contour integrals that have been transformed to a real integral ranging from 0 to ∞[52] and the Lewis integral[53] with the same limit. On the other hand, the four-body ionization amplitude contains only two-dimensional integrals with one contour integral and the Lewis integral. Thus, the dimension of the transition amplitude is reduced compared with our previous work.[41] Therefore, the present computations are very fast and economical in time relative to other theories. Finally, all the real integrations are carried out numerically by the Gauss quadrature method.

3. Results and discussion

In general, there are three common geometries for ion–atom or ion–molecule collisions that may be used to calculate the TDCS. From the TDCS results we study the collision dynamics in different kinematical regimes. In this context, we mention that Ren *et al.*[54,55] have studied the angular distributions of the ejected electron by calculating the TDCS in different collision planes. The coplanar geometry or scattering plane (x–z plane) (Fig. 1(a)) is defined by the incoming proton of momentum $\boldsymbol{k}_0$ (with energy E_0) and the outgoing electron of momentum $\boldsymbol{k}_{\rm e}$ (with energy $E_{\rm e}$) always being in the same x–z plane. In this plane, the scattered proton and the ejected electron are detected. However, in the perpendicular plane, the scattered proton is still on the scattering plane, while the ejected electron is detected on the y–z plane (shown in Fig. 1(b)). In the third plane, the so-called azimuthal plane, the scattered proton also remains in the scattering plane and the ejected electron is in the x–y plane as in Fig. 1(c).

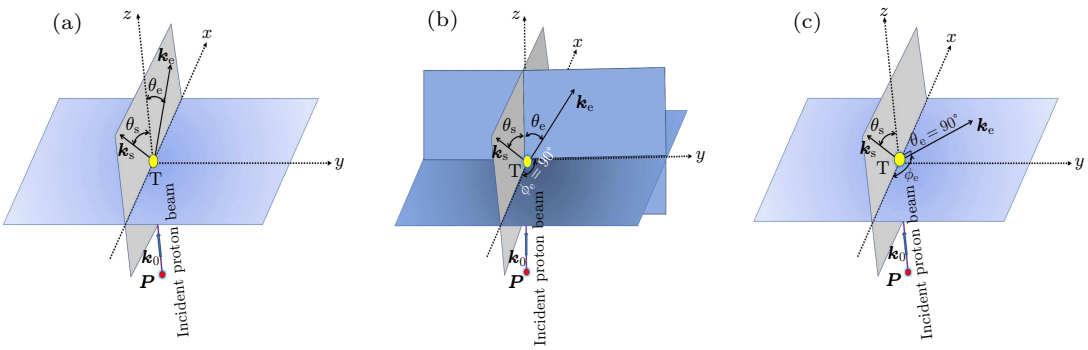


Fig. 1. The x–z, y–z and x–y planes represent (a) the scattering plane, (b) the perpendicular plane and (c) the azimuthal plane. The momentum of the incident projectile, scattered projectile and the emitted electron are $\boldsymbol{k}_0$, $\boldsymbol{k}_{\rm s}$ and $\boldsymbol{k}_{\rm e}$, respectively.

To check the validity of 3CW-3B and 3CW-4B as well as other theoretical calculations, we have calculated the TDCS and TDCS multiplied by $|\sin\theta_e|$, named TDCS*, as a function of the polar and azimuthal angles of the ejected electron for several electron emission energies (E_e) and momentum transfers ($\boldsymbol{q}$). The results are displayed in Figs. 2–5, respectively. We compare the theoretical values given by the 3CW, 2CW and FBA distorted wave models based on the three-body formalism, respectively, and the four-body formalism of the three-Coulomb wave (3CW-4B) with available experimental data. In the present work, we use the four-parameter wavefunction of Byron and Joachain[56] for the ground state of the He target He($1s^2$). It is given by

$$\phi_{\rm He}(\boldsymbol{r}_1,\boldsymbol{r}_2)=\frac{N}{4\pi}(A\,{\rm e}^{-\alpha r_1}+B{\rm e}^{-\beta r_1})(A\,{\rm e}^{-\alpha r_2}+B{\rm e}^{-\beta r_2}), \quad (8)$$

where $N=4\left[\frac{A^2}{\alpha^3}+\frac{B^2}{\beta^3}+\frac{16AB}{(\alpha+\beta)^3}\right]^{-1}$, with $A=2.60505$, $B=2.08144$, $\alpha=1.41$, $\beta=2.61$ and binding energy $\varepsilon_i=-2.86167$ a.u. This wavefunction $\phi(\boldsymbol{r}_1,\boldsymbol{r}_2)$[56] includes the static correlations that are of a spectroscopic nature. Conversely, a dynamic correlation is present in the perturbation potential that causes the transition to a collision. Here the function $\phi(\boldsymbol{r}_1,\boldsymbol{r}_2)$ is independent of angle. Therefore it includes radial correlations not angular correlations. We also use the simplest uncorrelated one-parameter wavefunction of Hylleraas[57]

$$\phi_{\rm He}(\boldsymbol{r}_1,\boldsymbol{r}_2)=\left(\frac{\alpha^3}{\pi}\right){\rm e}^{-\alpha(r_1+r_2)}, \quad (9)$$

where $\alpha=1.6875$ is the effective charge for He with binding energy $\varepsilon_i=-2.847656$ a.u.

In the present investigation, we focus our work on these geometries (shown in Figs. 1(a)–1(c)) in ion–atom collisions. In coplanar and asymmetric geometry, several theoretical as well as experimental works have been done at intermediate and high impact energies. Among these the agreement is quite good on the scattering plane. However, in the case of the perpendicular and azimuthal planes, few theoretical works have been found for p–He collisions. Since there are not sufficient experimental data in the literature for different kinematic parameters and different collision planes, we only present the theoretical TDCS results. The main features of the electron emission pattern are the presence of the well-known strong binary and weak recoil peaks. The binary peak is oriented roughly along the direction of momentum transfer $\boldsymbol{q}$, thus corresponding to electrons emitted after a single binary collision with the projectile. During the binary collision, the passive electron and the target ion are considered as spectators. In the opposite direction to $\boldsymbol{q}$, the recoil peak is found to arise due to a two-step classical double-scattering mechanism. So, this weak peak is mainly governed by strong elastic scattering from the nucleus.

Figures 2(a)–2(l) show the TDCS results in coplanar and asymmetric geometry for the ionization of a He atom by 1 MeV proton impact. We choose three momentum transfers $q=0.5$ a.u., 1 a.u. and 1.75 a.u. due to the availability of experimental data[18] (filled circles). For each value of $\boldsymbol{q}$, the ejected electron of energy E_e is chosen at 2.5 eV, 5 eV, 10 eV and 20 eV. Our theoretical calculations are compared with the experimental results[18] and the other theoretical calculations using the wave-packet convergent close-coupling approach (WP-CCC)[28] (orange curve). These figures also include the results obtained by the same 3CW-4B approach using the correlated wavefunction of Byron and Joachain[56] (violet curve) for the ground state of the He atom along with our 2CW-3B (blue curve) and FBA-3B (red curve) models. The result obtained by the distorted wave four-body (DW-4B)[49] (dash-dotted magenta curve) is also included in the same figure. This result exhibits better agreement with the experiment. On the other hand, both the 3CW-4B results using correlated and uncorrelated wave functions underestimate the measurement. This may be due to the fact that in the DW-4B model the incoming projectile is described by a Coulomb distorted wave while that for 3CW-4B is described by a plane wave. A comparison between the present 3CW-3B (black curves) results, the more successful WP-CCC (orange curve) model and the experimental data shows that all are in excellent agreement for all kinematical parameters. This is expected in the 3CW model, because the final state wavefunction incorporates distortions due to the pairwise Coulomb interaction. This wavefunction is asymptotically correct when all interparticle separations are large. It is also noted that all the particles in the final state are treated on an equal footing. Furthermore, in the entrance channel of the three-body formalism, the relative motion between the projectile and the target is described by the Coulomb distorted wave $\chi_i^+(\boldsymbol{R})$ in Eq. (4). On the other hand, the WP-CCC is a semi-classical two-center formalism in which the total scattering wavefunction is expanded on the basis of target-centered continuum pseudostates. This approximation incorporates the coupling between channels and multiple scattering. From these figures, it is also found that the 3CW-4B results using the correlated wavefunction[56] (violet curve) are slightly lower than the 3CW-3B results in the region of the binary peak, while the two sets (3CW-3B and 3CW-4B) of results follow exactly the same pattern. This is obvious because the bound electronic state of He^+ in the 3CW-4B model does not affect the dynamics at high impact energy where the frozen core approximation is valid. At the same time, FBA-3B (red curve) and 2CW-3B (blue curve) do not agree well with the experimental findings because neither theory accounts for the PI interaction. It is noted that the importance of PI interaction for single ionization of an atom was verified in earlier work.[3,6,8,49] The bound electron wavefunction of He^+

$(n = 1)$ and the perturbation potential is different in the three-body formalism than in the four-body formalism. Moreover, the treatment for the target wavefunction in the initial channel is completely different from the four-body model. These are the reasons for the discrepancies between the two sets of results (i.e., the three- and four-body formalisms). Therefore, a comparison of the TDCS results using the two-electron wavefunction and one active electron wavefunction of He in the ground state affects the results in the region of the binary peak. For all the considered values of low momentum transfer and at three different electron emission energies, the experimental data[18] show a double-peak structure: a large binary peak near the $\boldsymbol{q}$ direction and a smaller recoil peak in the vicinity of $-\boldsymbol{q}$, while the momentum transfer is low (shown in Figs. 2(a)–2(f)). But, in the case of high momentum transfer $q = 1.75$ a.u.

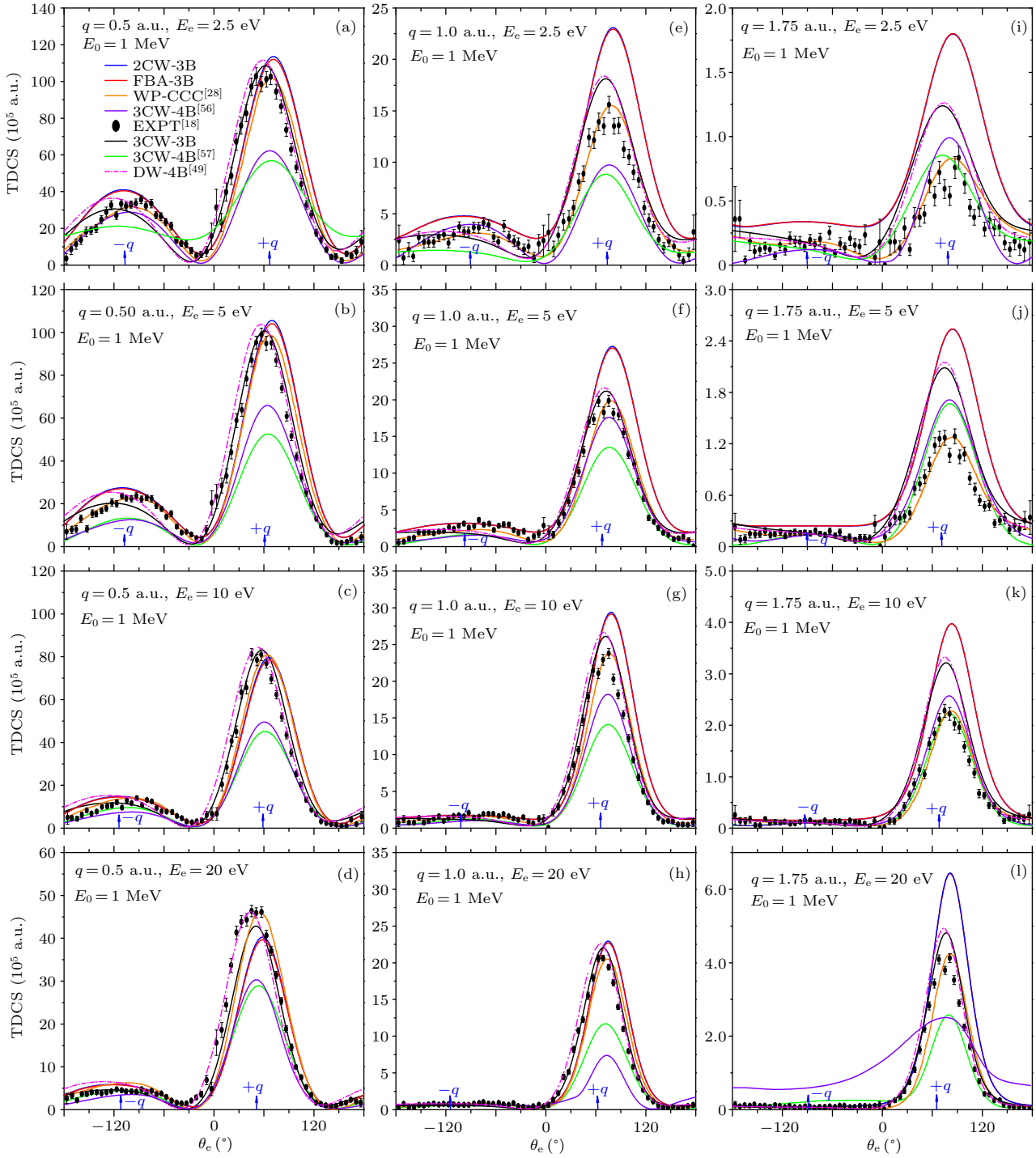


Fig. 2. Triple differential cross sections for single ionization of He in the ground state by 1 MeV proton impact in the scattering plane as a function of electron emission angle for three sets of electron emission energies and momentum transfers, as indicated in each figure. The green curve, black curve, blue curve and red curve represent the present 3CW-4B (uncorrelated wavefunction[57]), 3CW-3B, 2CW-3B and FBA-3B calculations, respectively. The orange curve is for WP-CCC,[28] the violet curve for 3CW-4B using a correlated wavefunction[56] and the dash-dotted magenta curve for DW-4B.[49] The filled circles show experimental results.[18]

and other sets of E_e, a single binary peak is observed. This structure was also obtained in earlier works.[21,22,28,29] Therefore, we can say that the double-scattering mechanism is insignificant compared with single scattering, while the projectile momentum transfer is high. Again, the height of the binary peak decreases with increasing momentum transfer. This is due to the interaction between the projectile and target ion and the projectile and electron. As also seen from these figures, the maximum discrepancy between the two curves using uncorrelated (green curve) and correlated (violet curve) wavefunctions of He in the 3CW-4B model occurs in the binary peak region. This means that in the binary peak region, the static electronic correlation has a significant influence on the ionization process, while in the other angular region the difference between the two curves is marginal. It is also noted that the binary peak shifts towards the smaller emission angle with increasing electron emission energy at a fixed value of projectile momentum transfer. This is due to projectile–electron interaction in the final state, i.e., the PCI effect. After direct ionization, the projectile attracts the outgoing electron and distorts the trajectory of that electron in a forward direction. The figures also show the results obtained using the 2CW-3B calculations, where the Coulomb distortion due to the relative motion between two nuclei is ignored in the final state. The results are exactly the same for FBA-3B. Some discrepancies both in the position and absolute values of the TDCS have been found between 3CW-4B and FBA-3B. The reason for this is the absence of PCI and PI interactions in FBA-3B and only PI interaction in 2CW-3B. One can also see that, with increasing momentum transfer at fixed E_e, the position of the binary peak moves towards larger ejection angles. This is due to the change in the direction of the momentum transfer.

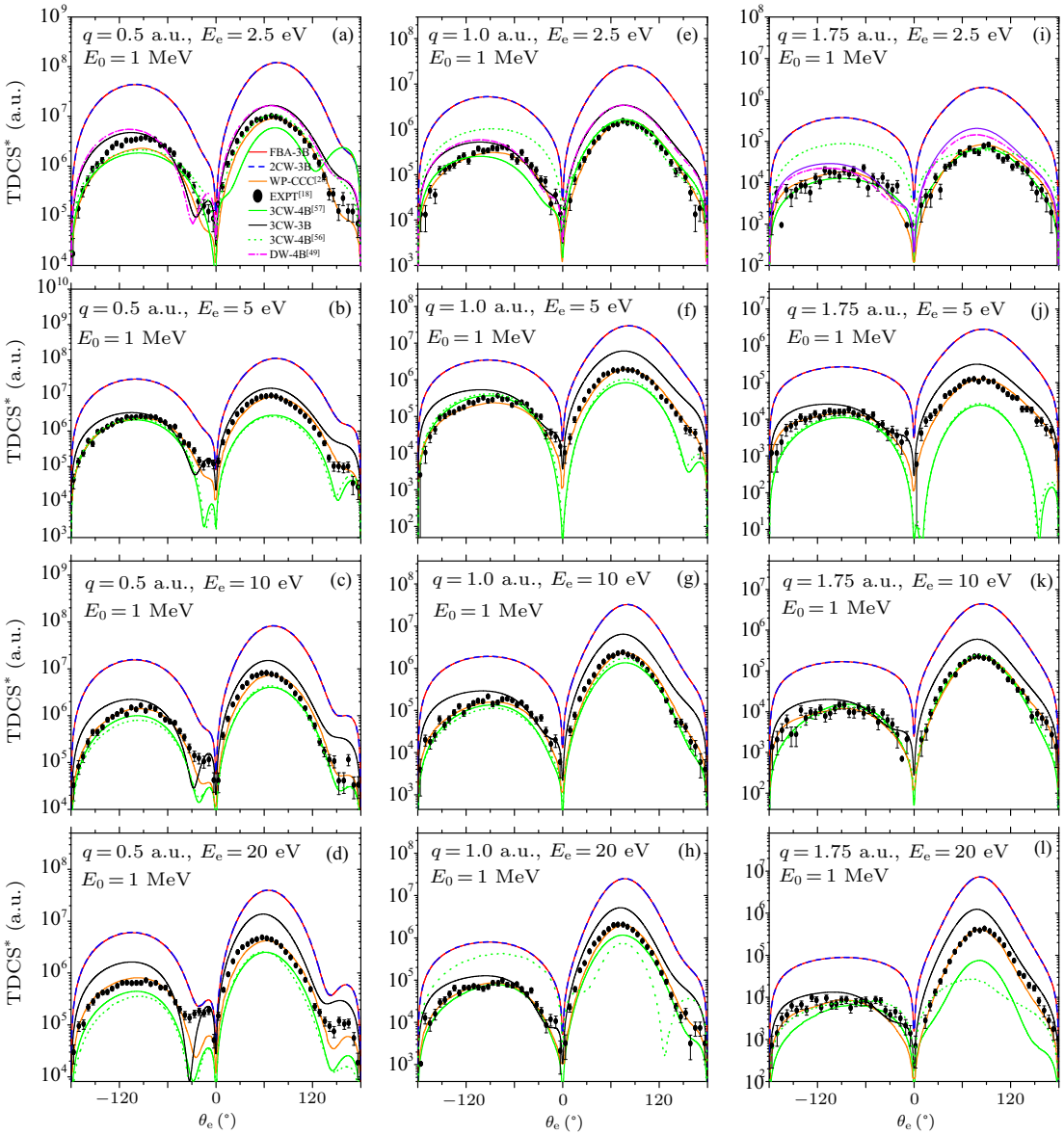


Fig. 3. TDCS* for 1 MeV proton impact ionization of He in the scattering plane as a function of electron emission angle for the electron emission energies and momentum transfers indicated in each figure. The green full and dashed curves, black curve, red curve, blue dashed curve and dash-dotted magenta curve represent the present 3CW-4B (uncorrelated and correlated wavefunction), 3CW-3B, FBA-3B and 2CW-3B and DW-4B calculations, respectively. The orange curve is for WP-CCC[28] and the filled circles show experimental data.[18]

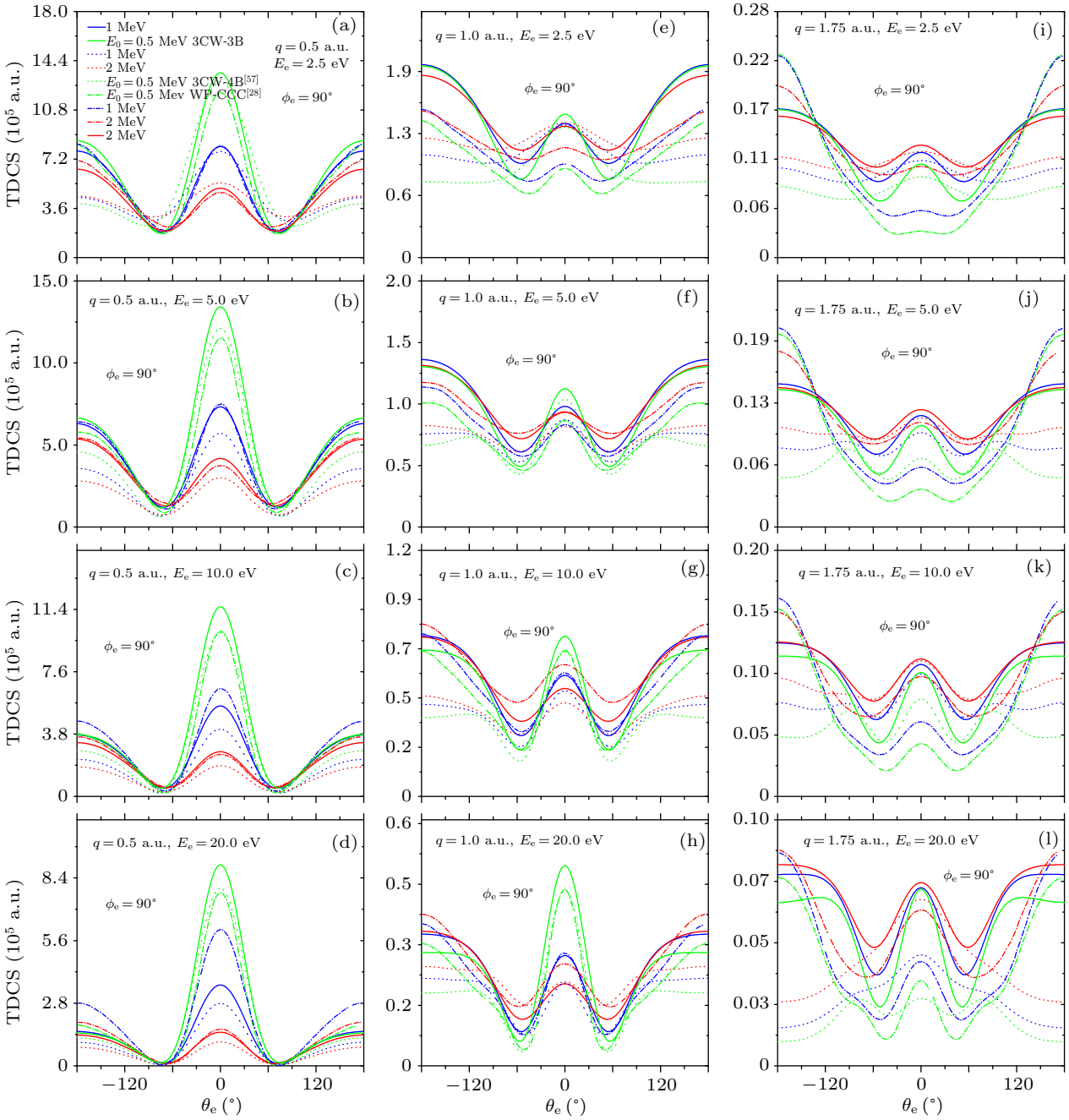


Fig. 4. Present TDCS results for single ionization of He by 0.5 MeV, 1 MeV and 2 MeV proton impact in the perpendicular plane as a function of electron emission angle for the electron emission energies and momentum transfers indicated in each figure. Full green, blue and red curves represent 0.5 MeV, 1 MeV and 2 MeV using 3CW-3B and the corresponding dotted curve obtained from 3CW-4B calculations using uncorrelated wavefunctions. The dash-dotted curve represents the WP-CCC results.[28]

In Fig. 3, we show the TDCS results multiplied by $|\sin\theta_e|$ (so-called TDCS*) for a proton impact energy of 1 MeV. Both the TDCSs (TDCS and TDCS*) produce equivalent information about the ionization process. The traditional TDCS form is used to study the binary and recoil peaks, as already discussed for Fig. 2. It is presented on a linear scale so that the shift of the peak is clearly seen among different models. On the other hand, TDCS* is presented on a logarithmic scale. A few comments should be made regarding the kinks in the TDCS* results near the forward and backward regions of the ejection angles. Kinks in the vicinity of 0° and 180° are found in TDCS* in which three nodes are present at 0° and ±180°. The kinks appear due to the asymmetry of the TDCS, which was mentioned in Ref. [18]. We note that the kinks appear in the 3CW-3B and 3CW-4B calculations using correlated and uncorrelated wave functions and WP-CCC[28] reproduces the experimental data.[18] But this type of structure is weak in the case of FBA-3B and 2CW-3B calculations. Moreover, we notice a relative angular shift (ranging from 0° to 10° in the direction of $\boldsymbol{q}$) of the experimental data with respect to our FBA-3B and 2CW-3B calculations for all kinematic conditions. The reason for such a shift is due to the absence of higher-order interaction terms as already mentioned in Ref. [15]. However, the other two models (3CW-

3B and 3CW-4B) agree comparatively better with the experimental findings. We should also remember that the structure disappears as projectile momentum transfer increases. Furthermore, 3CW-4B is in better agreement with the experiment than 3CW-3B, except for $E_e = 2.5$ eV and 5 eV at $q = 1.75$ a.u. We observe that the two sets of results using correlated (dotted green curve) and uncorrelated (solid green curve) wavefunctions do not exhibit a significant change in the angular distribution except for a few kinematic conditions. Again, we include the results in Figs. 3(a), 3(e) and 3(i) obtained with DW-4B[49] (dash-dotted magenta curve) model. We find good agreement with the experiment as well as the present 3CW-4B results. A description of the initial wave functions for DW-4B and 3CW-4B models has already been given. We must mention that for the DW-4B model the scattered projectile and ejected electron are described by the Coulomb distorted wave in the final state. However, in the 3CW-4B model, it is described by a three-Coulomb distorted wave due to the motion of three charged particles. The expressions for TDCS and TDCS* carry equivalent information and that for TDCS can be easily employed to understand its detailed angular distribution. On the other hand, TDCS* seems to be informative in places where measurements are hardly possible. This is evident from the sharp variation of our theoretical results around $\theta_e = 0^\circ$ and $\theta_e = 180^\circ$ (Figs. 3(a)–3(l)).

Figure 4 exhibits our TDCS results in the perpendicular plane for the same kinematic conditions as used in Fig. 2. There are no experimental data in the literature for these kinematic conditions so we present only the results obtained using our models (3CW-3B and 3CW-4B) and the WP-CCC results of Abdurakhmanov *et al.*[28] The TDCS in this plane is significantly smaller than the TDCS results for the scattering plane. For all the cases considered we see one strong binary peak at $\theta_e = 0^\circ$ and the other maximum is in the backward direction ($\pm 180^\circ$).

At $q = 0.5$ a.u., the height of the strong peak decreases with increasing electron emission energy. It is clear that the strong peak gets narrower and sharper with increasing electron emission energy. It is also noted that the relative difference in height between the strong peak and secondary peaks (at $\pm 180^\circ$) increases and the secondary peak height goes on diminishing compared with the strong peak as the electron emission energy increases. Good agreement between our models (3CW-3B and 3CW-4B) and WP-CCC is observed. One notable fact is that for a fixed electron emission energy, the TDCS curve with a lower impact energy (0.5 MeV) dominates over those with higher impact energies (1 MeV and 2 MeV).

For $q = 1$ a.u., we see a different picture of TDCS compared with that for $q = 0.5$ a.u. Here initially, at $E_e = 2.5$ eV, the secondary peak height is greater than the strong peak at 0°. However, with increasing electron emission energy the strong peak starts to dominate the secondary peaks and the dominance becomes most prominent for $E_e = 20$ eV. Other properties remain almost same as for $q = 0.5$ a.u.

In addition, there is a substantial difference between the two sets of results obtained with the three- and four-body formalisms. When the momentum transfer is increased to $q = 1.75$ a.u. (Figs. 4(i)–4(l)), the TDCS is maximum at 0° for a high impact energy (2 MeV); this is completely different (Figs. 4(a)–4(h)) for $q = 0.5$ a.u. and 1 a.u. This structure is found in both the calculations (3CW-3B and 3CW-4B). For a high value of $q = 1.75$ a.u., the sharp peak eventually separates into several peaks, especially in the 3CW-4B model with increasing electron energy. This feature may be a clear signature of the higher-order effects. This structure is not observed in our three-body formalism or the WP-CCC model.[28]

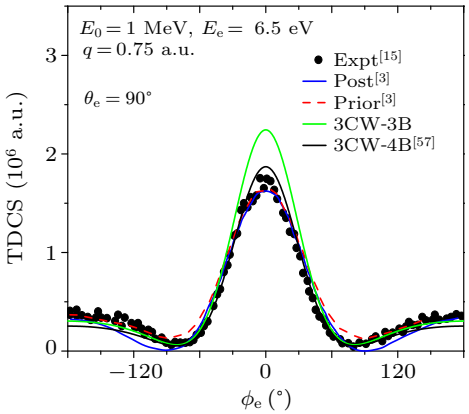


Fig. 5. TDCS for single ionization of He in the azimuthal plane by 1 MeV proton impact as a function of azimuthal ejection angles and for an ejected electron energy of 6.5 eV and $q = 0.75$ a.u. The black and green curves represent the results for 3CW-4B using uncorrelated wavefunctions and 3CW-3B. The blue curve (post) and dashed red curve (prior) show the CDW-4B results.[3] Filled circles are experimental results.[15]

Finally, we look at the electron emission spectrum in the azimuthal plane. Here, Fig. 5 shows our results for the TDCS. In this context, we mention that Gassert *et al.*[15] measured the TDCS (filled circles) in this plane at 1 MeV proton impact for an emission energy of 6.5 eV and momentum transfer $q = 0.75$ a.u. This figure also includes the results of Bidvari *et al.*[3] obtained by the post (blue curve) and prior (red dashed curve) forms of the four-body continuum-distorted wave (CDW-4B) approximation. We find a good level of agreement for the binary peak, especially the prior form of CDW calculated with inter-nuclear interaction included (red curve). So it seems that the binary interaction between the projectile and ejected electron represents a significant role for this plane. On the other hand, the 3CW-4B version accurately predicts the shape and location of the binary peak, although the absolute value is slightly higher than the experiment in the binary region. Figure 6 exhibits our predictions in the azimuthal plane for other kinematic conditions where no experimental results are available in the literature. Both the calculations

(four-body, three-body) and WP-CCC results[28] show a single binary peak at 0° with two maxima on either side of the peak, similar to Fig. 5. In the 3CW-4B results using the correlated wave function we observe a fair agreement in the angular distribution of TDCS in all kinematic conditions except $q = 1.75$ a.u., $E_e = 2.5$ eV (Fig. 6(i)). The shape is not so sharp as in other figures. On the other hand, Fig. 6(l) seems to have a bit of an unusual structure. For an impact energy of 0.5 MeV (solid magenta curve) we see two additional weak peaks on either side of that at $\phi_e = 0°$. This may be the manifestation of a higher-order effect that is also prominent in the perpendicular plane (Fig. 4(l)). One can see that with increasing momentum transfer (for a fixed electron emission energy), the two maxima on either side of the peak diminish and are almost flat for $q = 1.75$ a.u. A strong peak is found at 0°, which is similar to the results in the perpendicular plane. The results are larger at higher impact energies, i.e., in the azimuthal plane the cross sections become large for a high impact energy. Moreover, as the ejection energy and momentum transfer increase, the binary to recoil peak ratio increases again until the recoil peak eventually disappears. Thus, no recoil peak is found at $q = 1$ a.u. and 1.75 a.u. for all sets of ejection energies.

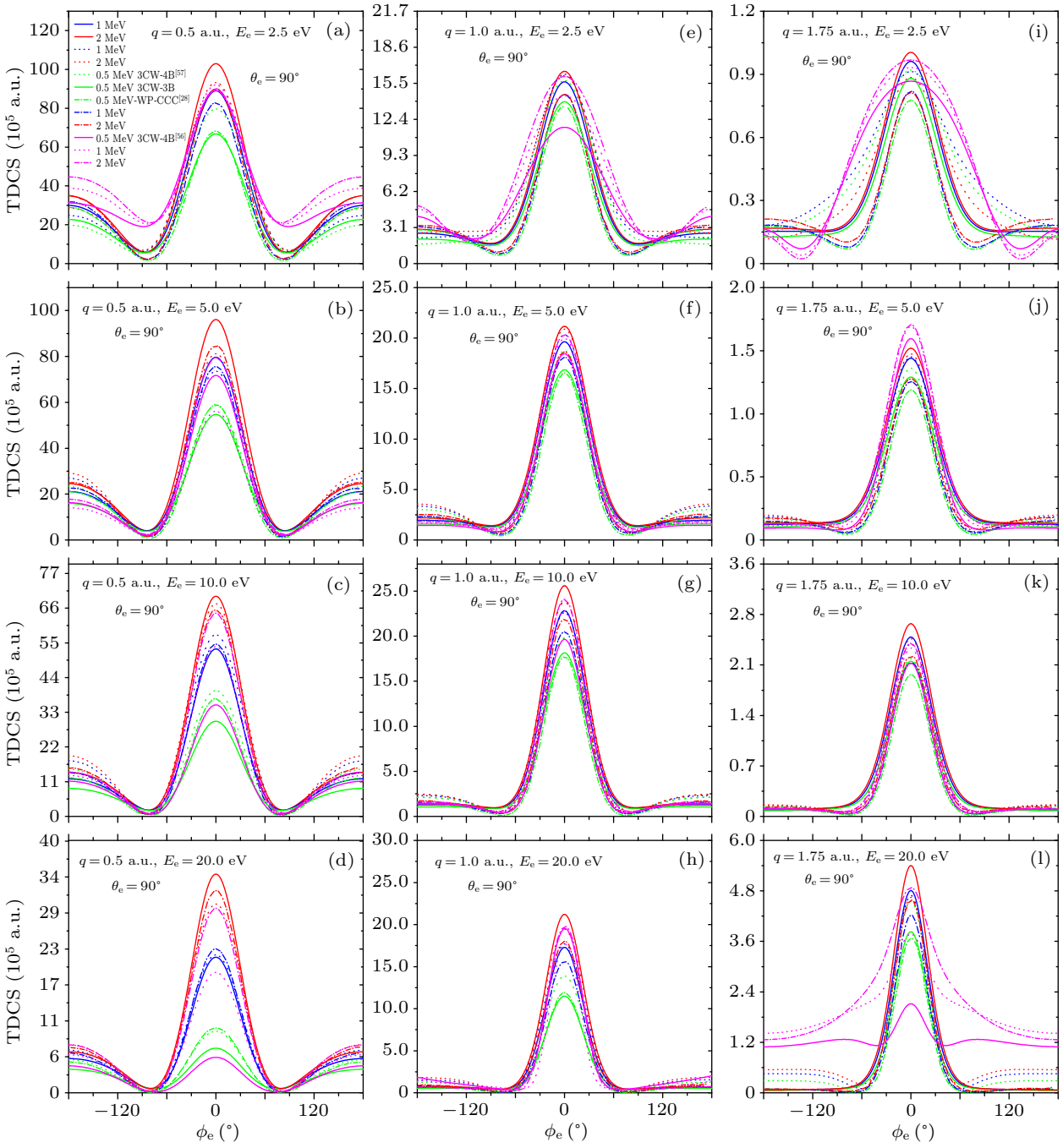


Fig. 6. The calculated TDCS for single ionization of He by 0.5 MeV (green curve), 1 MeV (blue curve) and 2 MeV (red curve) proton impact using 3CW-3B (full curve) and the corresponding dotted curve obtained from 3CW-4B calculations using uncorrelated wavefunctions. The dash-dotted curve represents the results of the WP-CCC model.[28] For 3CW-4B calculations using correlated wavefunctions the solid, dotted and dash-dotted magenta curves represent the TDCS for for single ionization of He by 0.5 MeV, 1 MeV and 2 MeV proton impact, respectively.

4. Summary and conclusion

In conclusion, the electron emission spectra in the scattering, perpendicular and azimuthal planes for several kinematical conditions have been investigated using a distorted-wave model based on the three-body and four-body formalisms. For this study, we chose simple p–He collision due to the availability of experimental data. We find a good level of accuracy in DW-4B models compared with 3CW-3B and 3CW-4B. Again, 3CW-3B gives better results than 3CW-4B which exposes the accuracy of the frozen core approximation in the high-energy region. Other than the small shift of the peak in the binary region, FBA-3B and 2CW-3B models reproduce the structure which is in agreement with the experiment for TDCS*. Moreover, our models do not work well for high projectile momentum transfer due to the absence of polarization that was used in many studies for high projectile energies. Its use is based on the idea that the electric field due to the incoming projectile gives an instantaneous distortion of the passive electron. Therefore, the interaction of that electron with the projectile can be modified. In the scattering plane, an intense binary peak and weak recoil peak occur except for high momentum transfer. Clearly, kinks in the vicinity of 0° and 180° emission angles in the calculations of TDCS* are found in the forward and backward emission angles that are verified by the WP-CCC approximation as well as the experimental results. In the perpendicular and azimuthal planes, the strong peak position does not shift as kinematic parameters change. However, in the case of the azimuthal plane, the intensity ratio of the binary to recoil peak diminishes as the electron ejection energies and projectile momentum transfer increase. Finally, it should be remembered that the electron correlation of the initial state wavefunction affects the TDCS results, especially in the region of the binary peak.

Acknowledgement

Project supported by the Science and Engineering Research Board (SERB), New Delhi, India (Grant No. CRG/2022/001668).

References

[1] Feng L, Sun S, Duan Q and Jia X 2015 *Chin. J. Chem. Phys.* **28** 595
[2] Wang F J, Sun S Y, Niu X J and Jia X F 2017 *Europhys. Lett.* **119** 43001
[3] Amiri Bidvari S, Fathi R and Brunger M J 2022 *Eur. Phys. J. Plus* **137** 701
[4] Amiri Bidvari S and Fathi R 2021 *Eur. Phys. J. Plus* **136** 190
[5] Amiri Bidvari S and Fathi R 2021 *Eur. Phys. J. Plus* **136** 453
[6] Ciappina M F and Cravero W R 2006 *J. Phys. B: At. Mol. Opt. Phys.* **39** 2183
[7] Maydanyuk N V, Hasan A, Foster M, Tooke B, Nanni E, Madison D H and Schulz M 2005 *Phys. Rev. Lett.* **94** 243201
[8] Dey R and Roy A C 2006 *Phys. Lett. A* **353** 341
[9] Sun S Y, Zhao H J and Jia X F 2018 *Europhys. Lett.* **123** 23002
[10] Ullrich J, Moshammer R, Dorn A, Dörner R, Schmidt L P H and Schmidt-Böcking H 2003 *Rep. Prog. Phys.* **66** 1463
[11] Misra D, *et al.* 2009 *Phys. Rev. Lett.* **102** 153201
[12] Schulz M, Hasan A, Maydanyuk N V, Foster M, Tooke B and Madison D H 2006 *Phys. Rev. A* **73** 062704
[13] Laforge A C, Egodapitiya K N, Alexander J S, Hasan A, Ciappina M F, Khakoo M A and Schulz M 2009 *Phys. Rev. Lett.* **103** 053201
[14] Schulz M, *et al.* 2010 *Phys. Rev. A* **81** 052705
[15] Gassert H, Chuluunbaatar O, Waitz M, *et al.* 2016 *Phys. Rev. Lett.* **116** 073201
[16] Schulzet M, *et al.* 2013 *Phys. Rev. A* **88** 022704
[17] Fischer D, Moshammer R, Schulz M, Voitkiv A and Ullrich J 2003 *J. Phys. B: At. Mol. Opt. Phys.* **36** 3555
[18] Chuluunbaatar O, *et al.* 2019 *Phys. Rev. A* **99** 062711
[19] Schulz M, Moshammer R, Fischer D, Kollmus H, Madison D H, Jones S and Ullrich J 2003 *Nature* **422** 48
[20] Foster M, Madison D H, Peacher J L and Ullrich J 2004 *J. Phys. B: At. Mol. Opt. Phys.* **37** 3797
[21] Ganbari-Adivi E and Eskandari S 2015 *Chin. Phys. B* **24** 013401
[22] Ganbari-Adivi E and Eskandari S 2015 *Chin. Phys. B* **24** 103403
[23] Ciappina M F, Cravero W R and Schulz M 2007 *J. Phys. B: At. Mol. Opt. Phys.* **40** 2577
[24] Ciappina M F and Cravero W R 2008 *Nucl. Instrum. Meth. Phys. Res. B* **266** 555
[25] Purohit G, Singh P and Patidar V 2014 *J. Elect. Spect* **197** 50
[26] Campeanu R I and Whelan C T 2021 *Atoms* **9** 33
[27] Sarkadi L 2018 *Phys. Rev. A* **97** 042703
[28] Abdurakhmanov I B, Kadyrov A S, Alladustov Sh U and Bray I 2019 *Phys. Rev. A* **100** 062708
[29] Madison D, Schulz M, Jones S, Foster M, Moshammer R and Ullrich J 2002 *J. Phys. B: At. Mol. Opt. Phys.* **35** 3297
[30] Schulz M, Moshammer R, Fischer D and Ullrich J 2004 *J. Phys. B: At. Mol. Opt. Phys.* **37** 4055
[31] Harris A L, Madison D H, Peacher J L, Foster M, Bartschat K and Saha H P 2007 *Phys. Rev. A* **75** 032718
[32] Gulyas L, Egri S and Igarashi A 2019 *Phys. Rev. A* **99** 032704
[33] Ciappina M F and Cravero W R 2006 *J. Phys. B: At. Mol. Opt. Phys.* **39** 1091
[34] Abdurakhmanov I B, Bray I, Fursa D V, Kadyrov A S and Stelbovis A T 2012 *Phys. Rev. A* **86** 034701
[35] Brauner M, Briggs J S and Klar H 1989 *J. Phys. B: At. Mol. Opt. Phys.* **22** 2265
[36] Jia X, Shi Q, Chen Z, Chen J and Zu K 1997 *Phys. Rev. A* **55** 1971
[37] Purkait K, Mondal M, Haque A, Mandal B and Purkait M 2023 *J. Phys. B: At. Mol. Opt. Phys.* **56** 145201
[38] Jana S, Samanta R and Purkait M 2012 *Eur. Phys. J. D* **66** 243
[39] Foster M, *et al.*. 2004 *J. Phys. B: At. Mol. Opt. Phys.* **37** 1569
[40] Chuluunbaatar O, Zaytsev S A, Kouzakov K A, Galstyan A, Shablov V L and Popov Yu V 2017 *Phys. Rev. A* **96** 042716
[41] Jana S, Samanta R and Purkait M 2013 *Phys. Scr.* **88** 055301
[42] Pedlow R T, O'rourke S F C and Crothers D S F 2005 *Phys. Rev. A* **72** 062719
[43] Bellm S, Lower J, Bartschat K, Guan X, Weflen D, Foster M, Harris A L and Madison D H 2007 *Phys. Rev. A* **75** 042704
[44] Bellm S, Lower J, Weigold E, Bray I, Fursa D V, Bartschat K, Harris A L and Madison D H 2008 *Phys. Rev. A* **78** 032710
[45] Harris A L, Milum B and Madison D H 2011 *Phys. Rev. A* **84** 052718
[46] Harris A L and Morrison K 2013 *J. Phys. B: At. Mol. Opt. Phys.* **46** 145202
[47] Ghanbari-Adivi E and Velayali A N 2013 *J. Phys. B: At. Mol. Opt. Phys.* **46** 065204
[48] Harris A 2019 *Atoms.* **44** 7
[49] Jana D, Samaddar S, Purkait K and Purkait M 2021 *Eur. Phys. J. D* **75** 164
[50] Clementi E and Roetti C 1974 *At. Data. Nucl. Data Tables* **14** 177
[51] Mondal A, Mandal C R and Purkait M 2016 *Eur. Phys. J. D* **70** 16
[52] Mitra C and Sil N C 1976 *Phys. Rev. A* **14** 1009
[53] Lewis R R 1956 *Phys. Rev* **102** 537
[54] Ren X, *et al.* 2015 *Phys. Rev. A* **91** 032707
[55] Ren X, *et al.* 2016 *Phys. Rev. A* **93** 062704
[56] Byron F W and Joachain C J 1966 *Phys. Rev. Lett.* **16** 1139
[57] Hylleraas E A 1929 *Z. Phys.* **54** 347